J Fluoresc (2016) 26:1671–1678
DOI 10.1007/s10895-016-1857-5

ORIGINAL ARTICLE

Synthesis and Optical Characterization of Red-Emitting $BaTa_2O_6:Eu^{3+}$ Phosphors

Mustafa İlhan[1] · **Mete Kaan Ekmekçi**[2] · **Ayhan Mergen**[1] · **Cemalettin Yaman**[3]

Received: 9 February 2016 / Accepted: 14 June 2016 / Published online: 21 June 2016
© Springer Science+Business Media New York 2016

Abstract Undoped and Eu^{3+} doped $BaTa_2O_6$ phosphors were synthesized via solid state reaction method and characterized by using XRD, SEM-EDS and photoluminescence (PL) analyses. The XRD results revealed that the crystal structure of $BaTa_2O_6$ allowed up to 10 mol% levels of Eu^{3+} ions due to the TTB characteristic network of adjacent octahedrals. SEM-EDS analyses confirmed the formation of $BaTa_2O_6$ structure and $EuTaO_4$ secondary phase. $BaTa_2O_6$:Eu^{3+} phosphors exhibited orange and red emissions at 592.2 nm and 615.7 nm in the visible region respectively. The Commission Internationale d'Eclairage (CIE) chromaticity coordinates of the $BaTa_2O_6$:Eu^{3+} phosphors that excited at λ_{ex} = 400 nm ranged from orangish-red to pinkish-red depending on increasing Eu^{3+} concentration.

Keywords $BaTa_2O_6$ · TTB · Eu^{3+} · Phosphors · Photoluminescence

✉ Mustafa İlhan
mustafa.ilhan@marmara.edu.tr

[1] Department of Metallurgical and Materials Engineering, Marmara University, Göztepe Kampüsü, Kadıköy, 34722 İstanbul, Turkey

[2] Department of Chemistry, Marmara University, Göztepe Kampüsü, Kadıköy, 34722 İstanbul, Turkey

[3] Department of Metallurgical and Materials Engineering, Yıldız Technical University, Davutpaşa Kampüsü, 34220, Esenler, İstanbul, Turkey

Introduction

Over the last few decades rare earth (RE^{3+}) ion doped materials have been played an important role in modern lighting and display technology which have been used in the field of photonics such as sensors, solid state lasers, optical memories, display monitors, white light emitting diodes, X-ray imaging, optical amplifiers, up-converters, optic-electronics, magnetic-optic devices, etc. [1–4]. Among all RE^{3+} ions, trivalent europium (Eu^{3+}) has been widely investigated for the red emmiting phosphors due to it's characteristic $^5F_0 \rightarrow {}^5I_j$ (J = 0,1,2,3,4) band transitions. The luminescence spectra of Eu^{3+} ion usually presents broad bands with the emission color varying from ultraviolet to red depending on the different host materials [5–7] which was dominated around 610 and 630 nm.

$BaTa_2O_6$ compound has been studied recently due to its dielectric, photocatalytic and photoluminescence properties [8–13]. $BaTa_2O_6$ ceramic forms in $BaO–Ta_2O_5$ system and it has three polymorphs as orthorhombic low temperature form, tetragonal form with tungsten bronze (TTB) type structure and hexagonal high temperature form [11, 13]. These different polymorphs strongly affect the properties of $BaTa_2O_6$. For example, the photocatalytic activity for water splitting properties of $BaTa_2O_6$ were found to depend on the crystal form of $BaTa_2O_6$. So, the photocatalytic activity of $BaTa_2O_6$ with orthorhombic form is higher than the tetragonal and hexagonal form [10]. The dielectric properties of $BaTa_2O_6$ ceramic have been reported by several authors. The dielectric properties of $BaTa_2O_6$ ceramic have been reported by a few authors. Ichinose and Shimada [8] reported that $BaTa_2O_6$ ceramic has a permittivity of 70, Q_f (THz) of 2.1 and temperature coefficient of resonant frequency of +200 ppm/°C.

$BaTa_2O_6$ ceramic powders have been produced by using different techniques in the literature. Kato and Kudo [10] synthesized $BaTa_2O_6$ powders mostly in orthorhombic form and with small amount of the tetragonal phase using BaB_2O_4 flux. The hexagonal phase of $BaTa_2O_6$ was obtained by phase transition at 1720 K as the low-temperature form. Conventional solid-state method forms $BaTa_2O_6$ phase at 1000 °C after prolonged heating time of 24 h [14]. $BaTa_2O_6$ was produced by coprecipitation technique [14]. Barium and tantalum ions were precipitated by a mixture of ammonium oxalate and ammonium hydroxide solutions. Single phase $BaTa_2O_6$ powder with an average particle size of 70 nm was produced after heat treatment at 750 °C for 6 h. $BaTa_2O_6$ was also synthesized by mechano-chemical synthesis after 10 h of high energy ball milling [15, 16].

In this study, undoped and Eu^{3+} doped $BaTa_2O_6$ ceramic phosphors were synthesized by a solid state reaction method. Micro structural and optical characterizations of the powders were investigated in detail by using the XRD, SEM and spectrofluorometic analysis.

Materials and Methods

Undoped and ($0.5 \leq x \leq 30$ mol%) Eu^{3+} doped $BaTa_2O_6$ phosphor ceramics were synthesized by a solid state reaction method. For that reason, stoichiometric amounts of $BaCO_3$ with purity of 99 % (Sigma-Aldrich), Ta_2O_5 with purity of 99.9 % (Alfa Aesar) were used as starting materials in order to synthesize undoped $BaTa_2O_6$. Eu_2O_3 dopant with purity of 99.9 % (Alfa Aesar) was subsequently added to the powder mixture to obtain $BaTa_2O_6$:Eu^{3+} phosphor ceramics. All mixtures were homogenized in agate mortar with the addition of acetone. Then, powders were sintered at 1425 °C for 20 h under air atmosphere in a temperature gradient electric furnace.

The crystalline sizes and phase compositions of sintered powders were characterized by using X-ray diffractometer (XRD, Rigaku Corp., D-MAX 2200) under Cu-K_α radiation between 2θ = 15–60° at 2°/min with Ni filter. The crystallite sizes of $BaTa_2O_6$ compound were calculated by using MDI Jade 6.5 program. The average crystallite sizes of the powders were calculated using the Scherrer Formula (1) [17]:

$$D = \frac{k \cdot \lambda}{B \cdot cos\theta} \quad (1)$$

D symbolizes particle size (nm); k is a constant (taken as 0.9); the wavelength of CuK_α, $\lambda = 0.15406$; B is the full width at half maximum (rad.); θ is the angle (°) between incident and diffracted beams.

The morphology of the heat treated ceramic powders was investigated by using Scanning electron microscopy (SEM, JEOL Ltd., JSM-5910LV) equipped with Energy dispersive spectroscopy (EDS, OXFORD Industries INCAx-Sight 7274; 133-eV resolution 5.9 keV) after Au-Pd coating.

Photoluminescence (PL) measurements (excitations and emissions) were performed by using Luminescence Spectrofluorometer (Scinco floromaster-FS/2 model) with a Xe-arc lamp (150 W) as excitation source. All the measurements were performed at room temperature.

Results and Discussion

X-Ray Diffraction and SEM-EDS Analyses

Figure 1 shows XRD patterns of undoped and doped $BaTa_2O_6$ samples sintered at 1425 °C for 20 h. $BaTa_2O_6$ single phase (JCPDS card No.17–0793) was obtained up to 15 mol% Eu^{3+} doping concentration while $EuTaO_4$ secondary phase (JCPDS card No.24–0412) was detected at higher levels of Eu^{3+}. XRD

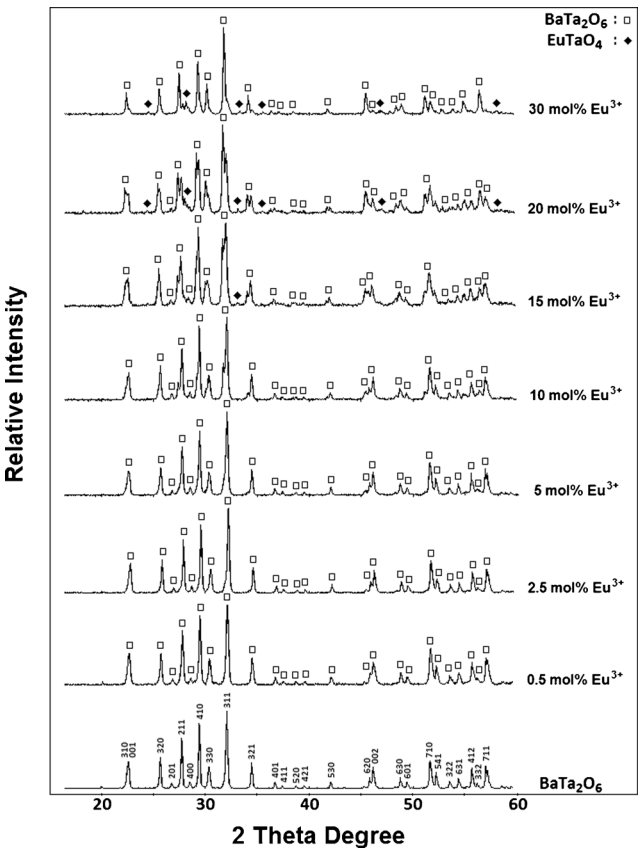

Fig. 1 X-ray diffraction patterns of undoped and Eu^{3+} doped $BaTa_2O_6$ structures between 0.5 to 30 mol%

analysis indicated that $BaTa_2O_6$ powders crystallized in tetragonal symmetry with space group *P4/mbm* having the tetragonal tungsten bronze (TTB) type structure. It was reported by Layden [18] that, $BaTa_2O_6$ has a tetragonal structure with cell parameters of $a = 12.52$ Å, $c = 3.956$ Å and $V = 620.10$ (Å)^3. TTB structure has the general formula of $A_2BC_2M_5X_{15}$, where X = O is anion, M = Ta is octahedral cation, and A, B and C are cations. A, B and C correspond to cationic sites with 15, 12 and 9 CN (coordination number), respectively [19]. TTB-$BaTa_2O_6$ structure has the pentagonal (A) sites and the square (B) sites which are occupied or not occupied by Ba^{2+} cations, while small triangular (C) sites have vacancies. All the polymorphs of $BaTa_2O_6$ that mentioned above can be described as the layers of corner-and edge-connected TaO_6 octahedra with Ba atoms which occupies the different types of tunnels parallel to the short axis [12]. Based on the ionic radius and valence, the square (B) sites in the structure might be occupied by smaller Eu^{3+} ions which have an ionic radius of 1.35 Å (12 of CN) [20] compared to Ba^{2+} ions, 1.61 Å (12 of CN)) [20]. Also, incorporation of Eu^{3+} ions may easily take place into the larger pentagonal (A) sites which were available for Ba^{2+} cations [20]. However, the vacant triangular (C) sites were too small to accommodate the Eu^{3+} cations.

The incorporation of RE^{3+} ions require charge compensation in the lattice structure. This aspect implies the formation of many non-equivalent optical centers. The one characteristic of TTB-type tantalates that the intra-octahedral distortion of the Ta^{5+} cation. This exhibits the off-center location of Ta^{5+} ions and the cooperative tilting of TaO_6 octahedra which induce a modulation of the $BaTa_2O_6$ structure. Consequently, a certain disorder in the orientation or in the shape of the coordination polyhedra occure. Accordingly, the crystal field around the RE^{3+} ions have been substantially perturbed, which leads to a significant inhomogeneous broadening of the absorption and emission peaks in the spectra [21]. Based on broadening in XRD patterns, a distortion in the lattice was also observed for the doping levels greater than 5 mol% and proved by the onset of diffraction peaks with increasing intensity indicating the slightly smaller angles for each of the main peaks in diffraction patterns. The lattice distortion might be a result of occupation of empty sites in the TTB structure by Eu^{3+} cations. This is similar to the pentagonal and square sites leading to a larger lattice constant to accommodate the presence of the dopants.

XRD revealed the average powder crystallite sizes along with the doping concentration which were found by Scharrer's equation. The crystallite size of undoped powder was around 41 nm after 20 h of sintering time. The crystallite size decreased with increasing Eu^{3+} concentration and varied from 40 nm to 27 nm for doping levels of 0.5 and 30 mol% respectively. Average crystallite size and the standard deviation of seven reflections were given in Table 1. Figure 2 (a-g) shows the SEM micrographs for undoped and 0.5, 2.5, 5, 10, 15 and 20 mol% Eu^{3+} doping concentrations respectively. The grain size decreased with increasing Eu^{3+} concentration and varied from submicron to a few microns for all powders. The grains exhibited nearly round and cornered shapes for powders. Consequently, both grain size and crystallite size decreased with increasing Eu^{3+} doping concentration. This situation may be attributed to the lattice distortion which suppressed the crystallite size and grain growth [22, 23]. SEM-EDS analysis of the 30 mol% Eu^{3+} doped powder is shown in Fig. 3(a-c). SEM micrograph (Fig. 3a) and EDS spectra (Fig. 3b and Fig. 3c) revealed the differences in the elemental composition of $BaTa_2O_6$:Eu^{3+} and $EuTaO_4$ structures.

Based on the XRD and SEM results, the incorporation of Eu^{3+} ions did not change the single phase structure of $BaTa_2O_6$ up to 15 mol% concentration by affecting the charge compensation in the structure. Therefore, it can be claimed that, some Eu^{3+} ions in the pentagonal and square sites of TTB structure may replace with the Ba^{2+} cations due to Ba evaporation [9, 16]. Accordingly, the change in the lattice distortion decreased with the increasing doping concentrations above 15 mol% due to the presence of $EuTaO_4$ phase. Hence, the narrowing peaks in XRD pattern of 30 mol% doped sample showed a relaxation in the lattice.

Photoluminescence Analysis

Spectral profile of barium tantalate host material exhibited a broad excitation band around 250 nm wavelenght where charge-transfer absorption of tantalates is possibly induced by weak interactions between TaO_6 octahedrals. The excitation peak has been attributed to the O^{2-}–RE^{3+} charge transfer band (CTB). Additionaly, edge-shared TaO_6

Table 1 Average crystallite size and standard deviation of Eu^{3+} doped $BaTa_2O_6$ powders

Eu^{3+} concentration (%)	Average crystallite size (nm)	Standard deviation
Undoped	38.43	1.69
0.5	36.92	1.93
2.5	35.33	1.87
5	33.01	1.74
10	30.75	1.55
15	25.12	1.92
20	24.37	1.65

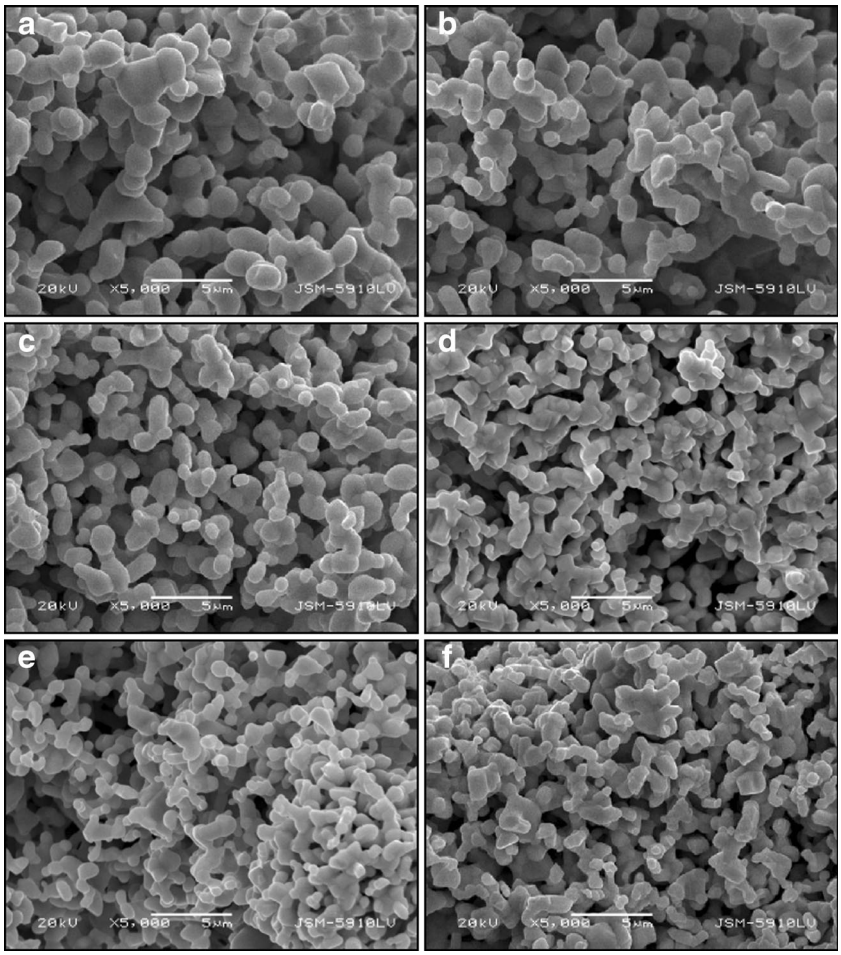

Fig. 2 SEM (seconder electron) micrographs at ×5000 magnification of Eu^{3+} doped $BaTa_2O_6$ structures at **a** 0.5 mol%, **b** 2.5 mol%, **c** 5 mol%, **d** 10 mol%, **e** 15 mol%, and **f** 20 mol%

groups are the efficient luminescent centres for the host emission which attributed to self-trapped excitation recombination [24]. Accordingly, the CTB transition in the $BaTa_2O_6$ host may lead to an electron transfer from ligand O^{2-} ($2P^6$) orbital to the empty state of $4f^6$ in the RE^{3+} ions.

Figure 4 shows the excitation spectra of $BaTa_2O_6$:xEu^{3+} ($0.5 \leq x \leq 30$ mol%) phosphors with emission monitored at 615.7 nm. The excitation spectra in the 350–500 nm range belongs to the transitions between the ground level $^7F_0$ and the excited levels $^5D_4$, ^5G_J, $^5L_6$, $^5D_3$, $^5D_2$ respectively. It was observed five excitation bands as $^7F_0 \rightarrow {}^5D_4$ (357.1 nm), $^7F_0 \rightarrow {}^5G_J$ (379.5 nm), $^7F_0 \rightarrow {}^5L_6$ (389.9 nm), $^7F_0 \rightarrow {}^5D_3$ (410.1 nm) and $^7F_0 \rightarrow {}^5D_2$ (464.6 nm) in the spectra. The assignments of the different excitation bands were identified on the basis of Dieke's energy level diagram [25]. Figure 4 also shows the CTB spectra of undoped and $BaTa_2O_6$:Eu^{3+} (x = 2.5, 5, 15 and 30 mol%) samples under 388.9 nm excitation wavelength. The broad excitation band at nearly 260 nm indicates that the charge transfer band (CTB) intensities of $BaTa_2O_6$:Eu^{3+} phosphors significantly changed depending on the dopant concentration. This interesting behaviour can be atributed to the crystal structure [26]. As it is seen from the Fig. 4 that the increasing dopant concentration significantly changed the CTB intensities for TTB-type structure. So, CTB peak intensity linearly increased up to 30 mol%.

Figure 5 shows emission spectra of $BaTa_2O_6$:Eu^{3+} phosphors excited at 389.9 nm. Spectrofluorometric analysis of $BaTa_2O_6$:Eu^{3+} phosphors exhibited two typical emission bands at 592.2 nm and at 615.7 nm due to $^5D_0 \rightarrow {}^7F_1$ and $^5D_0 \rightarrow {}^7F_2$ transitions, respectively. Luminescence intensity increased with increasing Eu^{3+} concentration up to 30 mol% and no concentration quenching has been observed. Figure 6 shows the magnetic ($^5D_0 \rightarrow {}^7F_1$) and electric dipol ($^5D_0 \rightarrow {}^7F_2$) band pass emissions with respect to the variation of Eu^{3+} doping concentration. Among Eu^{3+} ion transitions, it is well known that the $^5D_0 \rightarrow {}^7F_1$ magnetic dipole transition shows an orange color and hardly changes the crystal field strength around the Eu^{3+} ions. The $^5D_0 \rightarrow {}^7F_2$ electric dipole transition shows red color and the site symmetry of Eu^{3+} ions are very sensitive to the crystal field changes. As it's seen from the spectral profile, $^5D_0 \rightarrow {}^7F_1$ transition is weaker than the $^5D_0 \rightarrow {}^7F_2$ transition and emission intensity reached to

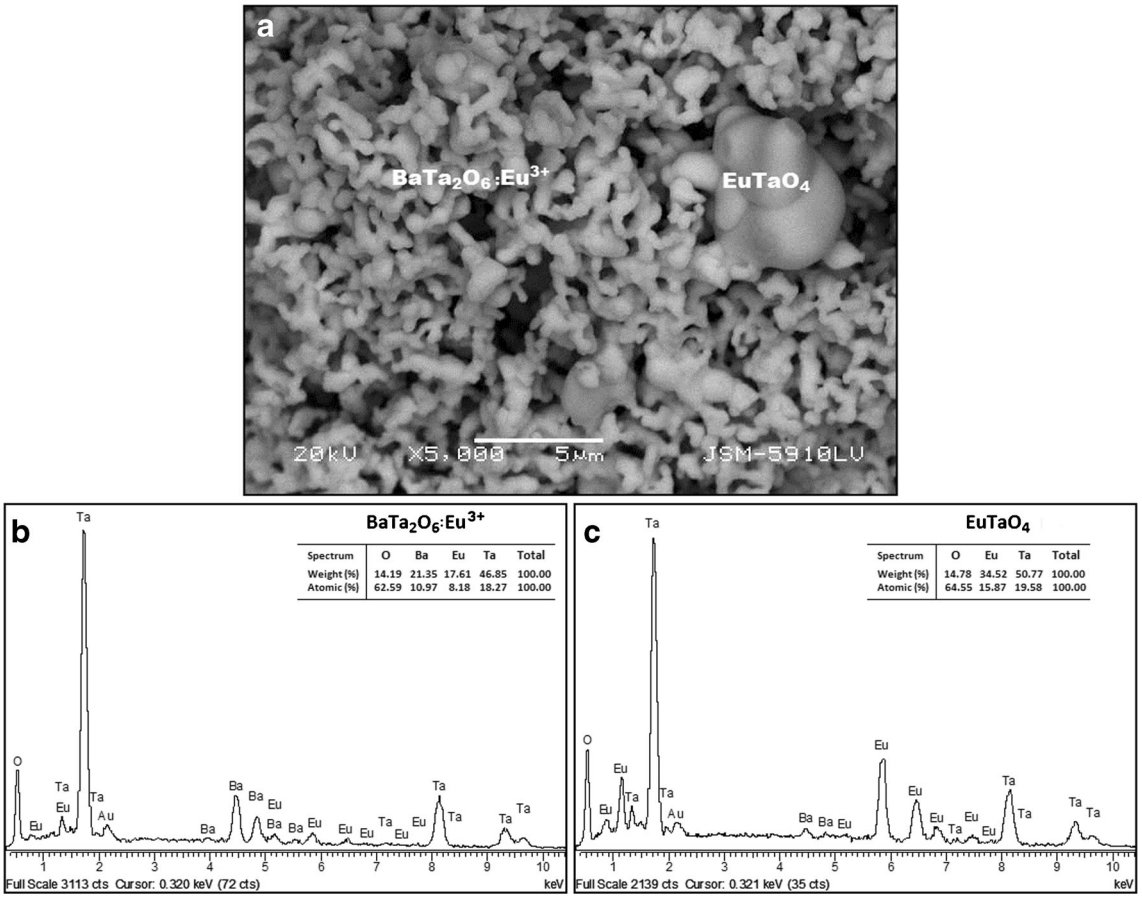

Fig. 3 **a** SEM (back scattering electron) micrograph at ×5000 magnification of Eu^{3+} doped $BaTa_2O_6$ structure, elemental analysis spectra and weight, atomic data of **b** Eu^{3+} doped $BaTa_2O_6$ grains at 30 mol% and, **c** $EuTaO_4$ phase

saturation level of the luminescence for the 20 mol% Eu^{3+} doping level. Consequently, emission intensity decreased for $^5D_0 \rightarrow {}^7F_1$ transition while remarkably increased for the $^5D_0 \rightarrow {}^7F_2$ transition above 20 mol%.

Figure 7 shows the asymmetry ratio (R) of the $BaTa_2O_6:Eu^{3+}$ phosphors depending on Eu^{3+} doping concentration. Asymmetry ratio (R) increased up to 30 mol% concentration and was 1.4 as a maximum R value for $BaTa_2O_6:Eu^{3+}$ phosphor. The ratio of

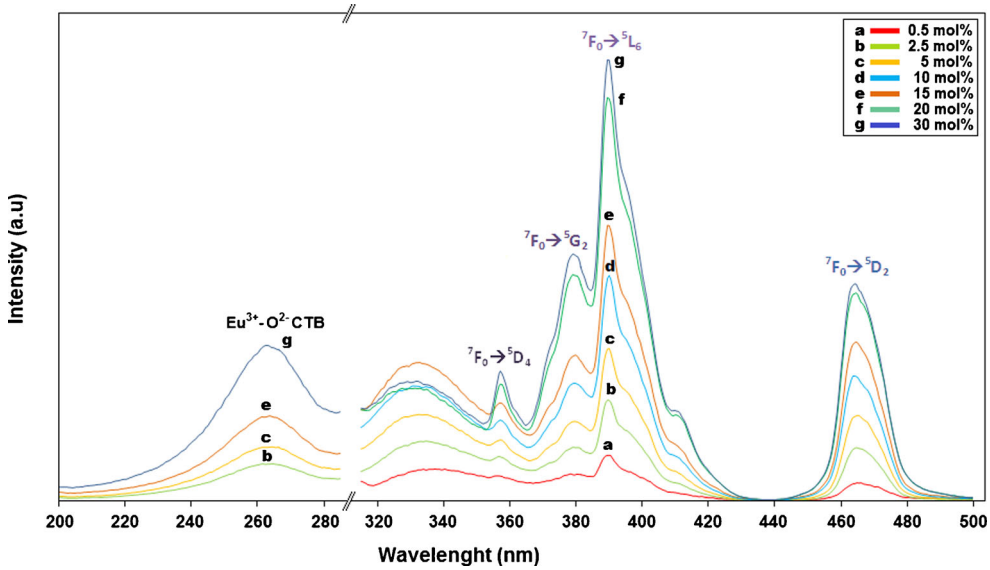

Fig. 4 Eu^{3+}– O^{2-} charge transfer band transitions at 389.9 nm, and excitation spectra of $BaTa_2O_6:Eu^{3+}$ monitored at 615.7 nm

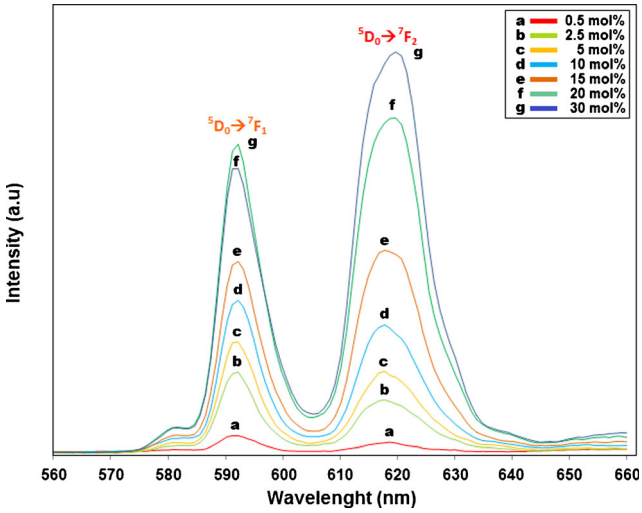

Fig. 5 Emission spectra of $BaTa_2O_6:Eu^{3+}$ monitored at 389.9 nm

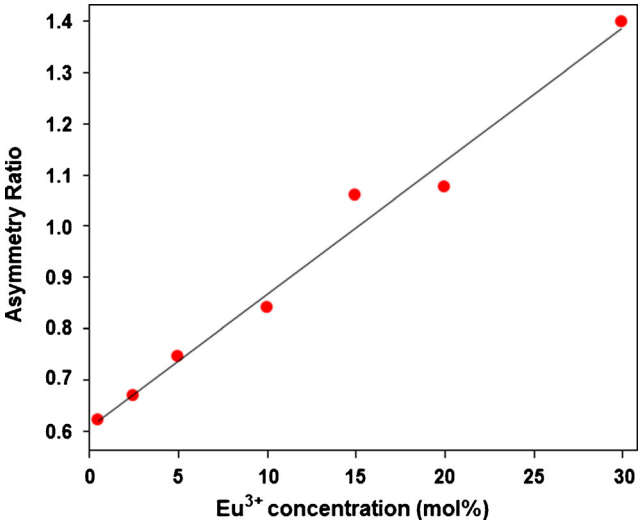

Fig. 7 Asymmetry ratio $BaTa_2O_6:Eu^{3+}$ as a function of Eu^{3+} concentration at 615.7 nm

electric dipole to magnetic dipole "($^5D_0 \rightarrow {}^7F_2$) / ($^5D_0 \rightarrow {}^7F_1$)" indicates the site symmetry of Eu^{3+} ions which is called as the asymmetry ratio (R). This ratio has been also used to explore the symmetry of the local environment of the RE^{3+} ions. Increasing of asymmetry ratio (R) indicated a decrease in the degree of covalency between europium and surrounding oxygen ions. In case of the location of Eu^{3+} cations into the non-centrosymmetric [27] pentagonal (A) sites with increasing doping levels, emission behavior of Eu^{3+} ions might be affected by the crystal field. On the other hand, when Eu^{3+} cations occupy the centrosymmetric [27] square (B) sites with increasing doping levels, emission will not affected by the crystal field. Hence, the change of coulomb attraction forces the activator (Eu^{3+}) to experience different crystal field, and lead to the red-shift on the emission spectra [28]. Moreover, increasing Eu^{3+} doping concentration up to 30 mol% caused a slightly shift of the emission peak from 617 to 620 nm. When the Eu^{3+} concentration reached 15 mol%, the second phase of the $EuTaO_4$ started to appear. The second phase $EuNbO_4$ aggregate would increase the Eu atoms occupying the noncentrosymmetric sites due to the forced electric dipole transition $^5D_0 \rightarrow {}^7F_2$ becoming hypersensitive [29]. The presence of $EuTaO_4$ may have also contributed the increasing of

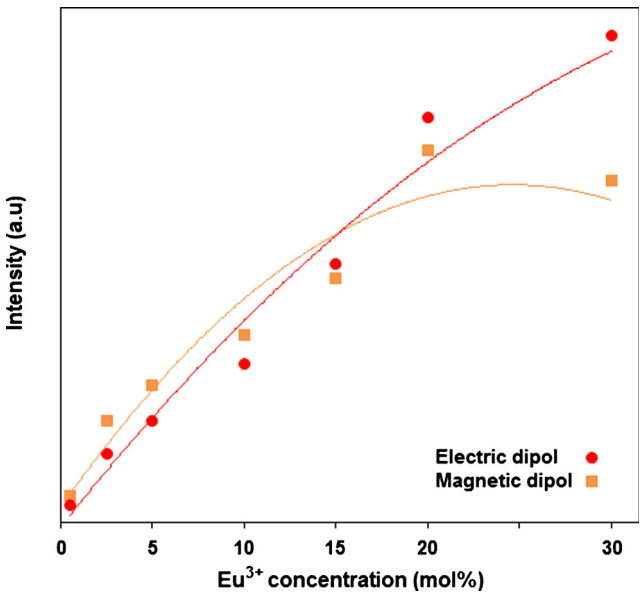

Fig. 6 Magnetic and electric dipole change as a function of Eu^{3+} concentration at 615.7 nm

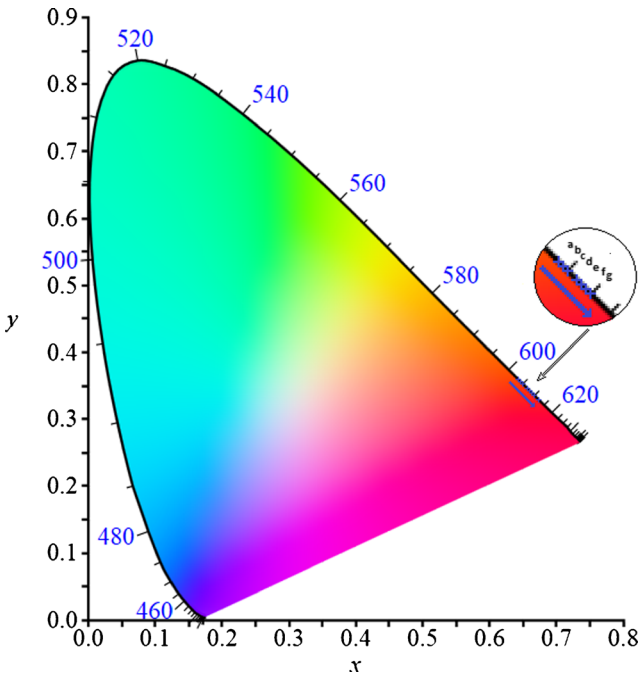

Fig. 8 The CIE chromaticity coordinate diagram of $BaTa_2O_6:Eu^{3+}$ phosphors

Table 2 CIE color coordinates of $BaTa_2O_6:Eu^{3+}$ at different Eu^{3+} concentrations under λ_{ex} = 389.9 nm

Sample	Eu^{3+} concentration (mol %)	CIE color coordinates	
		x	y
a	0.5	0.6408	0.3608
b	2.5	0.6458	0.3583
c	5	0.6492	0.3542
d	10	0.6575	0.3433
e	15	0.6608	0.3408
f	20	0.6621	0.3383
g	30	0.6645	0.3396

$^5D_0 \rightarrow {}^7F_2$ emission intensity and the asymmetric ratio. Based on the results, emission intensity of Eu^{3+} ions extensively increased due to the forced $^5D_0 \rightarrow {}^7F_2$ transition becoming hypersensitive [21, 30].

Figure 8 shows the CIE chromaticity diagram of $BaTa_2O_6:Eu^{3+}$ phosphors that varying with the Eu^{3+} ion content. The Commission Internationale de I'Eclairage (CIE) chromaticity coordinates of $BaTa_2O_6:Eu^{3+}$ phosphors were determined based on their corresponding PL spectra at a 389.9 nm or blue ray excitation. The CIE color coordinates were calculated as x = 0.6408, y = 0.3608 and x = 0.6645, y = 0.3396 for 0.5 and 30 mol% doping concentrations respectively, was presented in Table 2. The color coordinates shifted from an orangish red to a pinkish red depending on Eu^{3+} doping concentration.

Conclusions

Eu^{3+} doped TTB-type $BaTa_2O_6:Eu^{3+}$ phosphors were produced by conventional solid state method at 1425 °C for 20 h. XRD results revealed that the TTB single phase which formed between the 0.5 to 15 % Eu^{3+} doping concentrations. Also, a $EuTaO_4$ minor phase was observed above the 15 mol%. XRD and SEM results showed that, $BaTa_2O_6:Eu^{3+}$ crystallite and grain sizes decreased depending on Eu^{3+} concentration. $BaTa_2O_6:Eu^{3+}$ phosphors exhibited an orange emission at 592.2 nm and a red emission at 615.7 nm related to ($^5D_0 \rightarrow {}^7F_1$) and ($^5D_0 \rightarrow {}^7F_2$) band pass emissions respectively. Although red emission increased between 0.5 and 30 mol% doping concentrations, orange emission decreased above 20 mol% doped Eu^{3+}. Both the increase of Eu^{3+} ions at non-centrosymmetric A sites and the presence of $EuTaO_4$ minor phase might have affected the rise in asymmetry ratio (R). The results indicate that the $BaTa_2O_6:Eu^{3+}$ ceramic phosphor might be a good candidate for red emmiting LEDs.

References

1. Başak AS, Ekmekçi MK, Erdem M, Ilhan M, Mergen A (2016) Investigation of Boron-doping effect on photoluminescence properties of $CdNb_2O_6$: Eu^{3+} phosphors. J Fluoresc. doi:10.1007/s10895-015-1759-y
2. Moura AP de, Oliveira LH de, Paris EC, Li MS, Andrés J, Varela JA, on Longo E, Rosa ILV (2011) Synthesis, structural and Photophysical properties of $Gd_2O_3:Eu^{3+}$nanostructures prepared by a microwave sintering process. J Fluoresc, 21:1431–1438.
3. Faulques E, Wery J, Dulieu B, Seybert C, Perry DL (1998) Synthesis, fabrication, and photoluminescence of CaF_2 doped with rare earth ions. J Fluoresc 8:283–287
4. Vishwnath V, Srinivas M, Patel NP, Modi D, Murthy KVR (2016) J Fluoresc 26:277–282
5. Wang J, Song H, Kong X, Peng H, Sun B, Chen B, Zhang J, Xu W, Xia H (2003a) Fluorescence properties of trivalent europium doped in various niobate codoped glasses. J Appl Phys 93:1482
6. Wang Z, Yuan D, Xu D, Lv M, Cheng X, Pan L, Shi X (2003b) Growth and optical properties of Eu^{3+}-doped $La_3Ga_5SiO_{14}$ single crystal. J Cryst Growth 255:348–352
7. Wang Y, Endo T, Xie E, He D, Liu B (2004) Luminescence properties of $Ca_4GdO(BO_3)_3$:Eu in ultraviolet and vacuum ultraviolet regions. Microelectron J 35:357–361
8. Ichinose N, Shimada T (2006) Effect of grain size and secondary phase on microwave dielectric properties of $Ba(Mg_{1/3}Ta_{2/3})O_3$ and $Ba([Mg, Zn]_{1/3}Ta_{2/3})O_3$ systems. J Eur Ceram Soc 26:1755–1759
9. İlhan M (2014) Synthesis, structure and photoluminescence properties of Ho^{3+} doped TTB-BaTa2O6 phosphors. Solid State Sci 38: 60–168
10. Kato H, Kudo A (1998) New tantalate photocatalysts for water decomposition into H_2 and O_2. ChemPhys Lett 295:487–492
11. Layden GK (1968) Dielectric and structure studies of hexagonal $BaTa_2O_6$. Mater Res Bull 3:349
12. Lee YH, Kim YS, Kim DH, Oh MH (2007) Conduction mechanisms in barium tantalates films and modification of interfacial barrier height. IEEE Trans Electron Devices 47:71–76
13. Mumme WG, Grey IE, Roth RS, Vanderah TA (2007) Contrasting oxide crystal chemistry of Nb and Ta: the structures of the hexagonal bronzes $BaTa_2O_6$ and $Ba_{0.93}Nb_{2.03}O_6$. J Solid State Chem 180: 2429–2436
14. Navale SC, Samuel V, Gaikwad AB, Ravi V (2007) A coprecipitation technique to prepare $BaTa_2O_6$. Ceram Int 33:297–299
15. İlhan M, Mergen A, Yaman C (2011) Mechanochemical synthesis and characterisation of $BaTa_2O_6$ ceramic powders. Ceram Int 37: 1507–1514
16. İlhan M, Mergen A, Yaman C (2013) Removal of iron from $BaTa_2O_6$ ceramic powder produced by high energy milling. Ceram Int 39:5741–5750
17. Cullity BD,. Stock SR (2001) Elements of X-ray diffraction. third ed., Prentice Hall, USA
18. Layden GK (1967) Polymorphism of $BaTa_2O_6$. Mater Res Bull 2: 533
19. Simon A, Ravez J (2006) Solid-state chemistry and non-linear tungsten bronzes materials. C R Chim 9:1268–1276
20. Speight JG (1999) Lange's handbook of chemistry, 16th edn. The McGraw-Hill Companies, New York
21. Zhu G, Ci Z, Ma C, Shi Y, Wang Y (2013) A novel red emitting phosphor of Eu^{3+} doped TTB-type niobate $NaSr_2Nb_5O_{15}$ for white LEDs materials. Res Bull 48:1995–1998
22. Sadiq I, Khan I, Aen F, Islam MU, Rana MU (2012) Influence of rare earth Ce^{3+} on structural, electrical and magnetic properties of Sr^{2+} based W-type hexagonal ferrite. Physica B 407:1256–1261

23. Xu J, Zou H, Li H, Li G, Gana S, Hong (2009) Influence of Nd^{3+} substitution on the microstructure and electromagnetic properties of barium W-type hexaferrit J. Alloys Compd 490:552
24. Srivastava AM, Ackerman JF, Beeers WW (1997) On the luminescence of $Ba_5M_4O_{15}$(M=Ta^{5+}, Nb^{5+}). J Solid State Chem 134:187–191
25. Dieke GH (1968) Spectra and energy levels of rare earth ions in crystals. Interscience Publishers, New York
26. Marciniak L, Hreniak D, Strek W (2014) Controlling luminescence colour through concentration of Dy^{3+} ions in $LiLa_{1-x}Dy_xP_4O_{12}$ nanocrystals J. Mater Chem C 2:5704–5708
27. Li G, Cheng L, Liao F, Tian S, Jing X, Lin J (2004) Luminescent and structural properties of the series $Ba_{6-x}Eu_xTi_{2+x}Ta_{8-x}O_{30}$ and $Ba_{4-y}K_yEu_2Ti_{4-y}Ta_{6+y}O_3$. J Solid State Chem 177:875–882
28. Chen XY, Liu GK (2005) The standard and anomalous crystal-field spectra of Eu^{3+} J. Sol State Chem 178:419–428
29. Te-Hua F, Yu-Jen H, ChangYee-Shin CY-H (2006) Photoluminescent characterization of $KNbO_3$:Eu^{3+}. Mater Chem Phys 100:418–422
30. Shionoya S, Yen WM (1999) Phosphor handbook. CRC Press, Boca Raton, Florida